

A Model Fusion Distributed Kalman Filter For Non-Gaussian Observation Noise

Xuemei Mao^a, Gang Wang^b, Bei Peng^{a,*}, Jiacheng He^a, Kun Zhang^a, Song Gao^a

^a*The School of Mechanical and Electrical Engineering, University of Electronic Science and Technology of China, Sichuan, Chengdu, 611731, China*

^b*The School of Information and Communication Engineering, University of Electronic Science and Technology of China, Sichuan, Chengdu, 611731, China*

Abstract

The distributed Kalman filter (DKF) has attracted extensive research as an information fusion method for wireless sensor systems (WSNs). And the DKF in non-Gaussian environments is still a pressing problem. In this paper, we approximate the non-Gaussian noise as a Gaussian mixture model and estimate the parameters through the expectation-maximization algorithm. A DKF, called model fusion DKF (MFDKF) is proposed against the non-Gaussian noise. Specifically, the proposed MFDKF is obtained by fusing the sub-models that are built based on the noise approximation with the help of interacting multiple model (IMM). Considering that some WSNs demand high consensus or have restricted communication, consensus MFDKF (C-MFDKF) and simplified MFDKF (S-MFDKF) are proposed based on consensus theory, respectively. The convergence of MFDKF and its derivative algorithms are analyzed. A series of simulations indicate the effectiveness of the MFDKF and its derivative algorithms.

Keywords: Wireless sensor networks, Information fusion, Distributed Kalman filter, Gaussian mixture model, Expectation maximization, Interacting multiple model

*Corresponding author

Email address: beipeng@uestc.edu.cn (Bei Peng)

1. Introduction

Wireless sensor networks (WSNs) are widely used in technical applications, such as environmental monitoring, target tracking, and multiagent system [1–5]. Fusion of multiple sensor data for state estimation is one of the fundamental functions of WSNs that has sparked significant study due to its enhanced performance and practicality [6–9].

Centralized Kalman filter (KF) is a straightforward fusion architecture that collects data from all sensor nodes into a central node for processing [10]. Centralized KF has the benefit of being able to use all available information to obtain the best estimation in the minimum mean square error (MMSE) sense. Its burdensome computational and communication requirements make it challenging to expand, which is a drawback. And when a node fails, the estimations of the entire network are adversely affected. To solve the problems, distributed Kalman filter (DKF) is proposed for complex sensor networks [11–13]. The distributed architecture sets an independent local Kalman filter (LKF) at each node and uses point-to-point communication with neighboring nodes only. This enhances the scalability, robustness, and flexibility of the system. Moreover, consensus is an important issue, especially for collaborative sensor networks [14]. Therefore, some consensus algorithms are applied to the distributed architecture to further improve the system’s robustness by reducing the difference between the estimations of each node [15–18].

The above studies are conducted assuming that the system noise satisfies the Gaussian distribution, and most of them are based on the MMSE criterion. In practical applications, the observation noise often presents non-Gaussian characteristics due to the complex environment, disturbances, and other uncertainties, [19–21]. It leads to poor robustness of the DKF state estimation based on the MMSE criterion [22–24]. To address the issue, a lot of research focuses on state estimation in non-Gaussian environments. Particle filtering is regarded as an effective approach to solve the state estimation of nonlinear and non-Gaussian systems, which can track the state of any noise distribution [25]. Some distributed particle filters (DPFs) are proposed based on different fusion methods [26–29]. The common challenge of DPFs is the heavy computational burden generated by the massive number of particles. In [30], the DKF algorithms are proposed by assuming that the process and observation noise obey the Student’s t distribution, which has less computation complexity. Such methods perform well in heavy tail

noise, but in complex non-Gaussian environments, their estimation accuracy degrades due to fixed parameters of Student's t distribution.

Recently, methods in information-theoretic learning (ITL) are introduced to the state estimation under the non-Gaussian environment [31–34]. The DKF algorithms in [35, 36] are proposed based on the maximum correntropy criterion (MCC) [37]. When the observation noise is non-Gaussian, they outperform the conventional DKF (CDKF) for it can reflect the higher-order moment information of the error data and adjust the estimation correspondingly. This kind of DKF based on ITL can flexibly adapt to different non-Gaussian noise environments. In ITL, the minimum error entropy (MEE) [38] criterion is better than MCC in dealing with complicated non-Gaussian noise. The distributed minimum error entropy Kalman filter (DMEEKF) [39] is proposed based on the MEE criterion to promote the algorithm's robustness in a non-Gaussian environment. Nevertheless, their performance may degrade when exposed to strongly impulsive noise.

In background-impulse Kalman filter (BIKF) [40], another solution for non-Gaussian noise is proposed. It approximates the complex non-Gaussian noise as a combination of a small Gaussian noise and a large one, which offers a more accurate noise estimation for the KF. The excellent performance of BIKF under the non-Gaussian environment proves that the noise obeys non-Gaussian distribution can be well approximated as a combination of Gaussian components. It inspires us to model the observation noise as several Gaussian components with different variances.

To enhance the estimation accuracy of DKF applied in some WSNs, the contribution of this work is shown as follows.

- (a) In this work, a model fusion DKF (MFDKF) is proposed and its computational complexity is analyzed. We approximate the observation noise as a Gaussian mixture model (GMM) [41, 42] and estimate its parameters utilizing the expectation maximization (EM) algorithm [43, 44]. Thus, the observation model of LKF at each node can be built as composed of sub-models with different fusion noises and probabilities. With the help of interacting multiple model (IMM) [45, 46], the sub-models are fused, which improved the estimation of DKF against the non-Gaussian noise.
- (b) To be applicable to some special WSNs, two derived algorithms of MFDKF are proposed by consensus theory. Some WSNs, such as multi-agent systems have high requirements for node consensus. Some WSNs have limitations in communication due to the specific working environment

or other unavoidable reasons, such as underwater WSNs. Consensus MFDKF (C-MFDKF) and simplified MFDKF are proposed for consensus enhancement and communication reduction, respectively.

- (c) Some analyses are given to illuminate the performance of the proposed MFDKF and its derived algorithms, including mean error analysis and mean-square error analysis.

The rest of this paper is shown as follows. Section 2 gives some preparatory knowledge of MFDKF and explains the design motivation. Section 3 covers the implementation of the MFDKF algorithm and the analysis of computational complexity. Two derived algorithms of MFDKF called C-MFDKF and S-MFDKF are presented in Section 4. The performance analysis of the algorithms is presented in Section 5. Simulations and conclusions are revealed in Section 6 and Section 7, respectively.

2. Preliminaries

2.1. Analysis of DKF

A linear system can be described as

$$\mathbf{x}(k) = \mathbf{A}(k-1)\mathbf{x}(k-1) + \mathbf{w}(k-1), \quad (1)$$

$$\mathbf{z}_n(k) = \mathbf{H}_n(k)\mathbf{x}(k) + \mathbf{v}_n(k). \quad (2)$$

Here, $\mathbf{x}(k) \in \mathbb{R}^{p \times 1}$ is the unknown state vector at time k , $\mathbf{z}_n(k) \in \mathbb{R}^{q \times 1}$ is the observation vector of node n , which is available in the moment k . The known $\mathbf{A}(k) \in \mathbb{R}^{p \times p}$ and $\mathbf{H}_n(k) \in \mathbb{R}^{q \times p}$ are severally stand for the state transition matrix and the observation matrix of node n .

Supposing $\mathbf{w}(k) \in \mathbb{R}^{p \times 1}$ and $\mathbf{v}_n(k) \in \mathbb{R}^{q \times 1}$ are uncorrelated white Gaussian noises, their corresponding covariance matrices are $\mathbf{Q}(k)$ and $\mathbf{R}_n(k)$, respectively.

The point of DKF is to take the information from neighboring nodes into consideration. Assume there is a node 1 in the WSN, whose neighbors are node 2, ..., n . Define the following matrix

$$\begin{aligned} \mathbf{z}_c(k) &= \text{col}(\mathbf{z}_1(k), \mathbf{z}_2(k), \dots, \mathbf{z}_n(k)), \\ \mathbf{H}_c(k) &= \text{col}(\mathbf{H}_1(k), \mathbf{H}_2(k), \dots, \mathbf{H}_n(k)), \\ \mathbf{v}_c(k) &= \text{col}(\mathbf{v}_1(k), \mathbf{v}_2(k), \dots, \mathbf{v}_n(k)), \end{aligned} \quad (3)$$

where $col(\cdot)$ is an operator that put all the elements into a column vector to formulate a new matrix. Then, a fusion LKF observation model of node 1 can be described as

$$\mathbf{z}_c(k) = \mathbf{H}_c(k) \mathbf{x}(k) + \mathbf{v}_c(k), \quad (4)$$

and the covariance matrix of fusion observation noise $\mathbf{v}_c(k)$ is obtained by

$$\mathbf{R}_c(k) = \text{diag}(\mathbf{R}_1(k), \mathbf{R}_2(k), \dots, \mathbf{R}_n(k)), \quad (5)$$

where $\text{diag}(\cdot)$ is an operator to create a diagonal matrix.

By applying the conventional KF to model (1) and (4), the iterations of LKF is summarized as

$$\bar{\mathbf{x}}(k) = \mathbf{A}(k-1) \hat{\mathbf{x}}(k-1), \quad (6)$$

$$\mathbf{P}(k) = \mathbf{A}(k-1) \mathbf{M}(k-1) (\mathbf{A}(k-1))^T + \mathbf{Q}(k-1), \quad (7)$$

$$\mathbf{S}_c(k) = \mathbf{H}_c(k) \mathbf{P}(k) (\mathbf{H}_c(k))^T + \mathbf{R}_c(k), \quad (8)$$

$$\mathbf{K}_c(k) = \mathbf{P}(k) (\mathbf{H}_c(k))^T (\mathbf{S}_c(k))^{-1}, \quad (9)$$

$$\bar{\mathbf{v}}_c(k) = \mathbf{z}_c(k) - \mathbf{H}_c(k) \bar{\mathbf{x}}(k), \quad (10)$$

$$\hat{\mathbf{x}}(k) = \bar{\mathbf{x}}(k) + \mathbf{K}_c(k) \bar{\mathbf{v}}_c(k), \quad (11)$$

$$\mathbf{M}(k) = (\mathbf{I} - \mathbf{K}_c(k) \mathbf{H}_c(k)) \mathbf{P}(k). \quad (12)$$

Where, $\mathbf{M}(k)$ is the error covariance matrix of state estimation $\hat{\mathbf{x}}(k)$ and $\mathbf{P}(k)$ is the error covariance matrix of one step prediction $\bar{\mathbf{x}}(k)$. $(\cdot)^T$ represents the transpose operation.

Utilizing equation (8), (9) and the matrix inversion lemma, equation (11) is rewritten as

$$\hat{\mathbf{x}}(k) = \boldsymbol{\alpha} \bar{\mathbf{x}}(k) + \boldsymbol{\beta} \mathbf{z}_c(k), \quad (13)$$

$$\boldsymbol{\alpha} = \mathbf{M}(k) (\mathbf{P}(k))^{-1}, \quad (14)$$

$$\boldsymbol{\beta} = \mathbf{M}(k) (\mathbf{H}_c(k))^T (\mathbf{R}_c(k))^{-1}. \quad (15)$$

From equation (13) we know that the estimation of state can be simplified as a combination of the one-step prediction $\bar{\mathbf{x}}(k)$ and the fusion observation $\mathbf{z}_c(k)$. Equation (14) and equation (15) show that the combination coefficient $\boldsymbol{\alpha}$ and $\boldsymbol{\beta}$ are dependent on the error covariance matrix of one step prediction $\mathbf{P}(k)$ and the covariance matrix $\mathbf{R}_c(k)$.

The above analysis reveals the principle of DKF. A large covariance matrix of observation noise suggests an inaccurate observation and should be weighted less in the state estimation. Similarly, a small covariance matrix of observation noise means a precise observation and should be weighted more in the state estimation. The accuracy of state estimation suffers in CDKF because the covariance matrix of observation noise is unchanging and its value deviates substantially from the true value when impulsive noise exists.

2.2. Non-Gaussian Observation Noises

While the observation noises are non-Gaussian, the performance of CDKF decreases due to the inaccurate $\mathbf{R}_n(k)$. In other words, the statistic $\mathbf{R}_n(k)$ used to calculate the weight matrix β differs greatly from the true value, which results in the poor state estimation of CDKF.

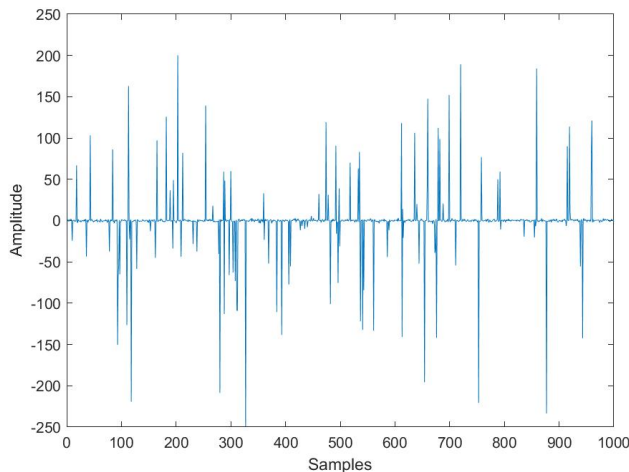


Figure 1: The mixed Gaussian noise

Take the mixed Gaussian noise shown in the Fig. 1 as an example, it obeys the distribution $v \sim 0.9N(0, 0.01^2) + 0.1N(0, 100^2)$. The statistic value of the covariance matrix is $\mathbf{R}_n(k) \approx 10^3$, which is larger than 0.01^2 and smaller than 100^2 . When there is no impulsive noise occurs, the observation is reliable, and the weight in the matrix β should be large, but a relatively smaller weight is used due to the relatively large covariance matrix of observation noise $\mathbf{R}_n(k)$. When the impulsive noise occurs, the observation becomes inaccurate, and the weight in the matrix β should become

smaller, but remains the relatively larger one due to the unchanged covariance matrix of observation noise $\mathbf{R}_n(k)$. In a word, as the inaccurate $\mathbf{R}_n(k)$ is used, the performance of the CDKF is poor.

In the DMCKF [35] and DMEEKF [39], the error between observation and predicted observation $\bar{\mathbf{v}}_n(k)$ (the calculation method refers to equation 10) are used to detect the occurrence of impulsive noise and adjust the weights accordingly. The issue is that even when no impulsive noise occurs and no weight adjustment is required, the weights are inaccurate. The reason is that the statistical estimation of the covariance matrix $\mathbf{R}_n(k)$ (which is used to calculate the weights) is inaccurate due to the presence of low-probability impulsive noise. Therefore, a more accurate covariance matrix of observation noise is expected in the non-Gaussian environment. It motivates us to approximate the non-Gaussian noise as a combination of several Gaussian components, which can help us to estimate the covariance matrix of observation noise in the non-Gaussian environment.

2.3. Approximation of non-Gaussian noise

The GMM is a linear combination of Gaussian noise, it allows the overall distribution of the observation noise to be divided into several Gaussian components. The probability density function is

$$p(\mathbf{v}(k)) = \sum_{i=1}^{\kappa} \gamma^i f(\mathbf{v}(k) | \boldsymbol{\mu}^i(k), \mathbf{R}^i(k)), \sum_{i=1}^{\kappa} \gamma^i = 1, \quad (16)$$

$$f(\mathbf{v}(k)) = \frac{\exp\left(\frac{1}{2}(\mathbf{v}(k) - \boldsymbol{\mu}^i(k))^T (\mathbf{R}^i(k))^{-1} (\mathbf{v}(k) - \boldsymbol{\mu}^i(k))\right)}{(2\pi)^{D/2} |\mathbf{R}^i(k)|^{1/2}}, \quad (17)$$

where $\mathbf{v}(k)$ is a D dimensional noise vector, $\boldsymbol{\mu}^i$ and $\mathbf{R}^i(k)$ severally denote the mean and covariance matrix of the i -th component. γ^i is the probability of the component i and $|\cdot|$ is the operator that calculates the determinant of a matrix.

Suppose there are ρ samples, the GMM parameters can be obtained from the following EM algorithm.

- (a) Initialize $\gamma^i(t)$, $\boldsymbol{\mu}^i$, and $\mathbf{R}^i(k)$, at $t = 0$.
- (b) Expectation step

$$w^i(k) = \frac{\gamma^i(t) f(\mathbf{v}(k) | \boldsymbol{\mu}^i(t), \mathbf{R}^i(t))}{\sum_{j=1}^{\kappa} \gamma^j(t) f(\mathbf{v}(k) | \boldsymbol{\mu}^j(t), \mathbf{R}^j(t))}, \quad (18)$$

(c) Maximization step

$$\gamma^i(t+1) = \frac{1}{\rho} \sum_{k=1}^{\rho} w^i(k), \quad (19)$$

$$\boldsymbol{\mu}^i(t+1) = \frac{\sum_{k=1}^{\rho} \gamma^i(k) \mathbf{v}(k)}{\sum_{k=1}^{\rho} \gamma^i(k)}, \quad (20)$$

$$\mathbf{R}^i(t+1) = \frac{\sum_{k=1}^{\rho} w^i(k) (\mathbf{v}(k) - \boldsymbol{\mu}^i(t))(\mathbf{v}(k) - \boldsymbol{\mu}^i(t))^T}{\sum_{k=1}^{\rho} w^i(k)}, \quad (21)$$

(d) Go back to step 2 until convergence.

In this paper, $\mathbf{v}(k)$ is the sample of observation noise, $k = 1, 2, \dots, \rho$. κ is the number of the Gaussian components, i.e. after the EM algorithm, the observation noise of each node can be divided into κ different Gaussian components. The covariance matrices of the Gaussian components at node n are denoted by

$$\{\mathbf{R}_n^1, \mathbf{R}_n^2, \dots, \mathbf{R}_n^\kappa\}, \quad (22)$$

$$\mathbf{R}_n^1 < \mathbf{R}_n^2 < \dots < \mathbf{R}_n^\kappa.$$

And their probabilities are denoted as

$$\{\gamma_n^1, \gamma_n^2, \dots, \gamma_n^\kappa\}, \quad \sum_{i=1}^{\kappa} \gamma_n^i = 1. \quad (23)$$

3. Proposed Model Fusion Distributed Kalman Filter

In this part, a model fusion DKF is designed. We first approximate the observation noise of each node as a GMM, and the specific parameters of the model are obtained by the EM algorithm described in Section 2.3. Then, the DKF observation model of node n can be approximated as a fusion of multiple sub-models. With the help of the IMM, a MFDKF is obtained by fusing sub-estimations given by sub-models. Besides, we modify the algorithm to address the anomalies in the application of the IMM method. Finally, the computational complexity of MFDKF is discussed.

3.1. Proposed MFDKF

Since the noise of each node is divided into κ Gaussian components, the observation model of each node can be divided into κ observation sub-models. Next, the observation model of DKF needs to be considered, which is obtained by fusing the observation models of each node and its neighbors. Akin to research in [36], a WSN with N nodes can be modeled as an undirected graph \mathcal{G} . Neighboring nodes refer to nodes that can communicate with each other. The adjacency matrix $\mathcal{A} = [a_{mn}] \in \mathbb{R}^{N \times N}$ is used to describe the neighbouring relations between nodes. If node m and node n can communicate with each other, then $a_{mn} = 1$, otherwise $a_{mn} = 0$. Self-edge is permitted, i.e., $a_{nn} = 1$. Define the degree of node n as $d_n = \sum_{n=1}^N a_{nm}$ representing the number of edges associated with node n .

The LKF observation model of node n is represented as

$$\mathbf{Y}_n(k) = \mathbf{C}_n(k) \mathbf{x}(k) + \mathbf{U}_n(k), \quad (24)$$

where,

$$\begin{aligned} \mathbf{Y}_n(k) &= [\mathbf{y}_1(k), \mathbf{y}_2(k), \dots, \mathbf{y}_{d_n}(k)]^T, \\ \mathbf{C}_n(k) &= [\mathbf{c}_1(k), \mathbf{c}_2(k), \dots, \mathbf{c}_{d_n}(k)]^T, \\ \mathbf{U}_n(k) &= [\mathbf{u}_1(k), \mathbf{u}_2(k), \dots, \mathbf{u}_{d_n}(k)]^T, \end{aligned} \quad (25)$$

the covariance matrix of fusion observation noise $\mathbf{U}_n(k)$ is denoted as

$$\mathbf{B}_n(k) = \text{diag}(\beta_1(k), \beta_2(k), \dots, \beta_{d_n}(k)). \quad (26)$$

The element in the above set is obtained from the neighbors of node n by the following operations.

- (a) Initialize: $m = 1, t = 1$.
- (b) Find the neighbor of node n : if $a_{mn} = 1$, then

$$\begin{aligned} \mathbf{y}_t(k) &= \mathbf{z}_m(k), \\ \mathbf{c}_t(k) &= \mathbf{H}_m(k), \\ \mathbf{u}_t(k) &= \mathbf{v}_m(k), \\ \beta_t(k) &= \mathbf{R}_m(k), \\ m &= m + 1, t = t + 1, \end{aligned} \quad (27)$$

else $m = m + 1$.

- (c) If $m \leq N$, return to step(b), else finish the operations.

Through the EM algorithm, each noise $\mathbf{u}_t(k)$ in the fusion observation model is divided into κ Gaussian components, which build the LKF observation sub-model as

$$\begin{aligned}\mathbf{Y}_n^j(k) &= \mathbf{C}_n(k) \mathbf{x}(k) + \mathbf{U}_n^j(k), \\ \mathbf{U}_n^j(k) &= \left[\mathbf{u}_1^{j1}(k), \mathbf{u}_2^{j2}(k), \dots, \mathbf{u}_{d_n}^{jd_n}(k) \right]^T,\end{aligned}\quad (28)$$

and the covariance of the j -th fusion noise $\mathbf{U}_n^j(k)$ is

$$\mathbf{B}_n^j(k) = \text{diag} \left(\beta_1^{j1}(k), \beta_2^{j2}(k), \dots, \beta_{d_n}^{jd_n}(k) \right). \quad (29)$$

The symbols $j1, j2, \dots, jd_n$ are used to denote the Gaussian component of the observation noise, and its value is an integer ranging from 1 to κ . For instance, $\mathbf{u}_n^{jt}(k)$ represents the jt -th Gaussian components of the noise $\mathbf{u}_n(k)$, whose covariance matrix and probability are $\beta_n^{jt}(k)$ and $\gamma_n^{jt}(k)$, respectively. $\mathbf{Y}_n^j(k)$ is the j -th LKF observation sub-model of node n .

It's necessary to note that the Gaussian noise $\mathbf{u}_n^{jt}(k)$ is not a real noise but a component obtained by approximating the real noise as GMM. Its covariance matrix and probability have been calculated by the EM algorithm. Accordingly, the LKF observation sub-model is not the true DKF observation model but a component acquired by fusing the observation sub-models of the node and its neighbors.

The IMM is a method that can deal with a system that has multiple models. Here, the observation model of LKF is approximated as multiple sub-models. In order to deal with these observation sub-models separately, the IMM is applied to the model (1) and (28). The number of LKF observation sub-models of node n is

$$L_n = \kappa^{d_n}. \quad (30)$$

The probabilities of the observation sub-models are calculated by

$$\begin{aligned}\alpha_n^j &= \gamma_1^{j1} \gamma_2^{j2} \dots \gamma_{d_n}^{jd_n}, \\ j &= 1, 2, \dots, L_n.\end{aligned}\quad (31)$$

The Markov transition probability matrix of node n is,

$$\tilde{\mathbf{P}}_n = \begin{bmatrix} \alpha_n^1 & \alpha_n^2 & \dots & \alpha_n^{L_n} \\ \alpha_n^1 & \alpha_n^2 & \dots & \alpha_n^{L_n} \\ \dots & \dots & \dots & \dots \\ \alpha_n^1 & \alpha_n^2 & \dots & \alpha_n^{L_n} \end{bmatrix}. \quad (32)$$

The element of $\tilde{\mathbf{P}}_n$ denoted as \tilde{P}_n^{ij} is the transition probability of node n from sub-model i to sub-model j .

Then, the steps of MFDKF run at each node are summarized as

(a) Initialization:

$$\begin{aligned}\chi_n^i(k-1) &= \alpha_n^i, \\ \hat{\mathbf{x}}_n^i(k-1) &= \mathbf{x}(0), \\ \mathbf{M}_n^i(k-1) &= \mathbf{M}(0),\end{aligned}\quad (33)$$

where $\chi_n^i(k-1)$ is the probability of the sub-model i at the instant $k-1$.

(b) Calculate the fusion probability:

$$\begin{aligned}\chi_n^{ij}(k-1) &= \tilde{P}_n^{ij} \chi_n^i(k-1) / \bar{c}_n^j, \\ \bar{c}_n^j &= \sum_{i=1}^{L_n} \tilde{P}_n^{ij} \chi_n^i(k-1).\end{aligned}\quad (34)$$

(c) Prepare the j -th fusion state based on sub-model j :

$$\hat{\mathbf{x}}_n^{pre-j}(k-1) = \sum_{i=1}^{L_n} \hat{\mathbf{x}}_n^i(k-1) \chi_n^{ij}(k-1). \quad (35)$$

(d) Prepare the error covariance matrix of the j -th fusion state:

$$\begin{aligned}\mathbf{M}_n^{pre-j}(k-1) &= \sum_{i=1}^{L_n} \chi_n^{ij}(k-1) \{ \mathbf{M}_n^i(k-1) + \\ & [\hat{\mathbf{x}}_n^i(k-1) - \hat{\mathbf{x}}_n^{pre-j}(k-1)] [\hat{\mathbf{x}}_n^i(k-1) - \hat{\mathbf{x}}_n^{pre-j}(k-1)]^T \}.\end{aligned}\quad (36)$$

(e) Perform the conventional KF for each sub-model:

$$\hat{\mathbf{x}}_n^j(k) = \bar{\mathbf{x}}_n^j(k) + \mathbf{K}_n^j(k) \bar{\mathbf{U}}_n^j(k), \quad (37)$$

where

$$\begin{aligned}\bar{\mathbf{x}}_n^j(k) &= \mathbf{A}(k-1) \hat{\mathbf{x}}_n^{pre-j}(k-1), \\ \bar{\mathbf{U}}_n^j(k) &= \mathbf{Y}_n^j(k) - \mathbf{C}_n(k) \bar{\mathbf{x}}_n^j(k), \\ \mathbf{K}_n^j(k) &= \mathbf{P}_n^j(k) (\mathbf{C}_n(k))^T (\mathbf{S}_n^j(k))^{-1}, \\ \mathbf{P}_n^j(k) &= \mathbf{A}(k-1) \mathbf{M}_n^{pre-j}(k-1) (\mathbf{A}(k-1))^T + \mathbf{Q}_n(k), \\ \mathbf{S}_n^j(k) &= \mathbf{C}_n(k) \mathbf{P}_n^j(k) (\mathbf{C}_n(k))^T + \mathbf{B}_n^j(k).\end{aligned}\quad (38)$$

(f) Obtain the error covariance of $\hat{\mathbf{x}}_n^j(k)$:

$$\mathbf{M}_n^j(k) = [\mathbf{I} - \mathbf{K}_n^j(k) \mathbf{C}_n(k)] \mathbf{P}_n^j(k). \quad (39)$$

(g) Calculate the likelihood function matched to sub-model j :

$$\Lambda_n^j(k) = \frac{\bar{c}_n^j}{\sqrt{2\pi |\mathbf{S}_n^j(k)|}} \exp\left(-\frac{1}{2}(\bar{\mathbf{U}}_n^j(k))^T (\mathbf{S}_n^j(k))^{-1} \bar{\mathbf{U}}_n^j(k)\right). \quad (40)$$

(h) Update the model probability:

$$\chi_n^j(k) = \frac{\Lambda_n^j(k)}{\sum_{i=1}^{L_n} \Lambda_n^i(k)}. \quad (41)$$

(i) Obtain the fusion state estimation of node n :

$$\hat{\mathbf{x}}_n(k) = \sum_{j=1}^{L_n} \chi_n^j(k) \hat{\mathbf{x}}_n^j(k). \quad (42)$$

3.2. Modification of the MFDKF

In the steps above, the likelihood function calculated from equation (40) may go to zero, when most of the neighboring nodes are subjected to strongly impulsive noise. As a result, the denominator in equation (41) tends to be zero, which leads to the collapse of iterations. A simple solution is to use $\chi_n^j(k) = \bar{c}_n^j$, when the strongly impulsive noise occurs. But, this modification will cause the algorithm to be unusually unstable, and the performance of its root mean square errors (RMSEs) are shown in Fig. 2.

Then, we suppose that all the neighboring nodes are suffered from the most impulsive noise when this abnormality occurs. At this point, the predicted fusion observation noise $\bar{\mathbf{U}}_n^j(k)$ is utilized to obtain a more precise fusion covariance matrix $\mathbf{B}_n^j(k)$, and the equation (41) is replaced by

$$\begin{cases} f \sum_{j=1}^{L_n} \Lambda_n^j(k) \sim 0 : \\ \left\{ \begin{array}{l} \chi_n^{j=\hat{j}}(k) = 1, \chi_n^{j \neq \hat{j}}(k) = 0, \\ \mathbf{B}_n^{j=\hat{j}}(k) = \bar{\mathbf{U}}_n^{j=\hat{j}}(k) \left(\bar{\mathbf{U}}_n^{j=\hat{j}}(k) \right)^T, \\ \hat{j} = j_{\max(\mathbf{B}_n^j(k))}. \end{array} \right. \\ \text{else} : \chi_n^j(k) = \Lambda_n^j(k) / \sum_{j=1}^{L_n} \Lambda_n^j(k). \end{cases} \quad (43)$$

Fig. 4a shows the RMSEs of the improved algorithm, which indicate that the corrective actions worked in eliminating the abnormal estimations.

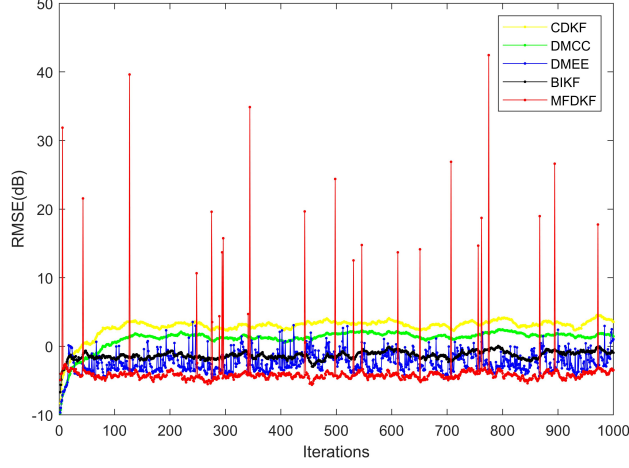


Figure 2: RMSEs of the abnormal algorithm

Remark 1. If there is only one node exists in the communication net, i.e., the sensor node has no neighbor, the distributed algorithm is the same as the conventional KF. And the proposed MFDKF is reduced to BIKF when the parameter $\kappa = 2$ and no communication occurs in the WSN.

3.3. Computational Complexity

In this part, the computational complexity of MFDKF is analyzed from the perspective of floating-point operations. Table 1 list the computational complexities of equations, where d denotes the degree of node n , and L denotes the number of observation sub-models. The computational complexity of the CDKF depends on equations (6)-(12) and that of the MFDKF depends on equation (31), (34)-(42). Correspondingly, the computational complexity of CDKF and MFDKF are respectively,

$$S_{CDKF} = 6p^3 + 6dp^2q + 4d^2pq^2 + dpq - p + O(d^3q^3), \quad (44)$$

$$S_{MFDKF} = \left(\begin{array}{l} 6p^3 + 6dp^2q + 4d^2pq^2 + 2d^2q^2 \\ + (4L - 1)p^2 + dpq + 3Lp + dq \\ + q + 4L + d + 3 + O(d^3q^3) \end{array} \right) L - p. \quad (45)$$

$O(\cdot)$ is the same term infinitesimal of the variable.

From [36], We can obtain the computational complexity of DMCKF

$$\begin{aligned} S_{DMCKF} &= (2\tau + 8)p^3 + (4\tau + 6)p^2dq + (2\tau - 1)p^2 \\ &+ (4\tau + 2)pd^2q^2 + (3\tau - 1)pdq + (4\tau - 1)p \\ &+ 2\tau d^3q^3 + 2\tau dq + \tau O(p^3) + 2\tau O(d^3q^3), \end{aligned} \quad (46)$$

where τ represents the average fixed-point iteration number of node n . According to [39], the computational complexity of DMEEKF is

$$\begin{aligned} S_{DMEEKF} &= (8\tau + 8)p^3 + 8\tau q^3 + (22\tau + 6)p^2q \\ &- (2\tau + 1)p^2 + (18\tau + 2)pq^2 + \tau q + (5\tau - 1)p \\ &+ (10\tau - 1)pq + \tau O(p^3) + \tau O(q^3) + \tau O(pq). \end{aligned} \quad (47)$$

L is calculated by equation (30), therefore the computational complexity of DMEEKF depends on κ and d . It's easy to see that the computation complexity of MFDKF is larger than CDKF. It is difficult to compare the computational complexity of MFDKF with that of DMCKF and DMEEKF directly. When the values of τ and L are of the same order of magnitude, it can be said that their computational complexity is of the same order of magnitude. We run these algorithms using MATLAB R2020a on an i5-12490F and 3.0 GHz CPU. The simulation results can be found in Fig.4a and Table 4a. From the average simulation time listed in Table 2, we can conclude that the computational complexity of the proposed MFDKF is slightly higher than that of DMEEKF in this example.

4. C-MFDKF and S-MFDKF Based on Consensus Fusion

In the MFDKF, the information exchanged between non-neighboring nodes is forbidden. There is no centralized information center to coordinate, and each node implements the LKF to obtain its state estimation. WSNs with high consensus requirements face challenges when applying MFDKF because nodes' estimations may not be consistent (close to each other).

For improvement, a C-MFDKF is proposed to reinforce the consensus between nodes. The consensus fusion rules are

$$\begin{aligned} \varphi_n(k) &= \mathbf{A}(k-1)\hat{\mathbf{x}}_n(k-1), \\ \hat{\mathbf{x}}_n^c(k) &= \hat{\mathbf{x}}_n(k) + \eta_n \sum_{m \in N_{ei_n}} (\varphi_m(k) - \varphi_n(k)), \end{aligned} \quad (48)$$

where η_n is the fusion gain of the node, $\hat{\mathbf{x}}_n^c(k)$ is the final estimation of node n after the consensus fusion. The form of the fusion gain is

$$\eta_n(k) = \frac{\xi}{d_n}, \quad (49)$$

where, ξ is a constant and $0 \leq \xi < 1$.

Table 1: Computational complexities of equations

Equation	+ and \times	Division, matrix inverse, Cholesky decomposition and exponentiation
(6)	$2p^2 - p$	0
(7)	$4p^3 - p^2$	0
(8)	$2dp^2q + 2d^2pq^2 - dpq$	$O(d^3q^3)$
(9)	$2dp^2q + 2d^2pq^2 - 2dpq$	0
(10)	$2dpq$	0
(11)	$2dpq$	0
(12)	$2p^3 + 2dp^2q - p^2$	0
(31)	$dL - L$	0
(34)	$3L^2 - L$	0
(35)	$2L^2p - Lp$	0
(36)	$4L^2p^2 - Lp^2 + L^2p$	0
(37)	$2dpqL$	0
(38)	$(4p^3 + p^2 + 4dp^2q + 4d^2pq^2 - dpq - p) L$	$LO(d^3q^3)$
(39)	$(2p^3 + 2dp^2q - p^2) L$	0
(40)	$(2d^2q^2 + dq + 1) L$	$4L + LO(d^3q^3)$
(41)	$L^2 - L$	L
(42)	$2Lp - p$	0

Table 2: Average simulation time of different algorithms

Filters	Average simulation time (s)
CDKF	0.0116
DMCKF	0.0305
DMEEKF	0.1917
BIKF	0.0101
MFDKF	0.2060

Here, the estimations of the neighboring nodes at the previous moment are used for local coordination at this moment, with the aim of converging the estimations of all the nodes in the WSN. The C-MFDKF is simply summarized as

- (a) LKF at each node: implement MFDKF as proposed in section 3.
- (b) Consensus fusion: update the estimations through the consensus fusion rules in equation (48), where the parameter η_n is calculated by equation

(49),

(c) Go back to step (a) continue the MFDKF steps.

Remark 2. When $\xi = 0$, the consensus term in C-MFDKF does not work and degenerates to MFDKF.

Actually, MFDKF and C-MFDKF are not suitable for WSNs with some limits in the information exchange between neighboring nodes, such as the WSN in the underwater environment. To reduce the information interaction in the algorithm, a simplified version of MFDKF is proposed based on the aforesaid consensus fusion rules.

In the S-MFDKF, each node implements the LKF with its own observation only. This means that no communication occurs during the LKF process. The consensus fusion rule described above is then applied to each node's estimation. This method intends to improve the accuracy of each LKF estimation by fusing the previous moment estimations of its neighbors. The S-MFDKF step is summarized as

(a) LKF at each node: implement the proposed MFDKF in section 3 in a communication-free way, i.e.

$$\begin{aligned} \mathbf{Y}_n(k) &= \mathbf{z}_n(k), \\ \mathbf{C}_n(k) &= \mathbf{H}_n(k), \\ \mathbf{B}_n(k) &= \mathbf{R}_n(k). \end{aligned} \tag{50}$$

(b) Consensus fusion: Update the estimations through the consensus fusion rules in equation (48), where the parameter η_n is calculated by equation (49),

(c) Go back to step (a) continue the MFDKF steps.

The communication contents of the proposed MFDKF and its derived algorithms are listed in Table 3, from which we can conclude that the S-MFDKF has the least amount of information interaction with its neighbors. Consequently, C-MFDKF is a good choice when the WSN communication capability is good. If a high level of consensus is not necessary, the MFDKF is the best option. And when the WSN communication capability is limited S-MFDKF should be applied.

Remark 3. The MFDKF, C-MFDKF, and S-MFDKF are equivalent when communication between nodes is prohibited.

Table 3: Communication contents between the node and its neighbor in proposed algorithm

Algorithm	MFDKF	C-MFDKF	S-MFDKF
Communication contents	$\mathbf{H}_n(k)$	$\mathbf{H}_n(k)$	
	$\mathbf{z}_n(k)$	$\mathbf{z}_n(k)$	$\hat{\mathbf{x}}_n(k)$
	$\mathbf{R}_n(k)$	$\mathbf{R}_n(k)$	
		$\hat{\mathbf{x}}_n(k)$	

5. Performance Analysis

In this part, several analyses are conducted to illuminate the performance of the proposed MFDKF and its derived algorithms, including mean error and mean-square error. The derivation is on the basis of the following assumptions:

1. The transition matrix and the observation matrix of the system are time-invariant, thus $\mathbf{A}(k) = \mathbf{A}$, $\mathbf{C}_n(k) = \mathbf{C}_n$.
2. State noise $\mathbf{w}(k)$ and observation noise $\mathbf{v}(k)$ are independent of each other, and their expectations are equal to zero.

5.1. Mean Error Analysis

The performance of mean error is reflected in the expectation of the estimation error $E\{\boldsymbol{\varepsilon}_n(k)\}$. Here, the discussion is divided into two parts, one is the essential MFDKF algorithm, and another is the consensus fusion rules that are applied in C-MFDKF and S-MFDKF.

Firstly, the MFDKF algorithm is considered. The estimation error of node n with the observation model j is calculated by

$$\boldsymbol{\varepsilon}_n^j(k) = \mathbf{x}(k) - \hat{\mathbf{x}}_n^j(k). \quad (51)$$

According to equation (42), the LKF estimation error of node n at time k is calculated by

$$\begin{aligned} \boldsymbol{\varepsilon}_n(k) &= \mathbf{x}(k) - \hat{\mathbf{x}}_n(k) \\ &= \mathbf{x}(k) - \sum_{j=1}^{L_n} \chi_n^j(k) \hat{\mathbf{x}}_n^j(k) \\ &= \sum_{j=1}^{L_n} \chi_n^j(k) \boldsymbol{\varepsilon}_n^j(k). \end{aligned} \quad (52)$$

Substitute equation (1), (28), (35), (37) and (38) into equation (51) obtain

$$\begin{aligned} \boldsymbol{\varepsilon}_n^j(k) &= \mathbf{f}_n^j(k) \mathbf{A} \sum_{i=1}^{L_n} \chi_n^{ij}(k-1) \boldsymbol{\varepsilon}_n^i(k-1) \\ &+ \mathbf{f}_n^j(k) \mathbf{w}(k-1) - \mathbf{K}_n^j(k) \tilde{\mathbf{v}}_n^j(k), \end{aligned} \quad (53)$$

where

$$\begin{aligned} \mathbf{f}_n^j(k) &= \mathbf{I} - \mathbf{K}_n^j(k) \mathbf{C}_n \\ &= \mathbf{I} - \mathbf{P}_n^j(k) (\mathbf{C}_n)^T \left(\mathbf{C}_n \mathbf{P}_n^j(k) (\mathbf{C}_n)^T + \mathbf{B}_n^j(k) \right)^{-1} \mathbf{C}_n \\ &= \left[(\mathbf{P}_n^j(k))^{-1} + (\mathbf{C}_n)^T (\mathbf{B}_n^j(k))^{-1} \mathbf{C}_n \right]^{-1} (\mathbf{P}_n^j(k))^{-1}. \end{aligned} \quad (54)$$

Then, the expectation of $\boldsymbol{\varepsilon}_n^j(k)$ is

$$E \{ \boldsymbol{\varepsilon}_n^j(k) \} = \mathbf{f}_n^j(k) \mathbf{A} \sum_{i=1}^{L_n} \chi_n^{ij}(k-1) E \{ \boldsymbol{\varepsilon}_n^i(k-1) \}. \quad (55)$$

It is known that

$$\begin{aligned} \left\| \sum_{i=1}^{L_n} \chi_n^{ij}(k-1) E \{ \boldsymbol{\varepsilon}_n^i(k-1) \} \right\| &\leq \\ \max \left[\|E \{ \boldsymbol{\varepsilon}_n^1(k-1) \}\|, \dots, \|E \{ \boldsymbol{\varepsilon}_n^{L_n}(k-1) \}\| \right], \end{aligned} \quad (56)$$

and denote the right of it as

$$\|E \{ \boldsymbol{\varepsilon}_n^m(k-1) \}\| = \max \left[\|E \{ \boldsymbol{\varepsilon}_n^1(k-1) \}\|, \dots, \|E \{ \boldsymbol{\varepsilon}_n^{L_n}(k-1) \}\| \right]. \quad (57)$$

Apply the inequation into equation (55) we have

$$E \{ \boldsymbol{\varepsilon}_n^j(k) \} \leq \mathbf{f}_n^j(k) \mathbf{A} \|E \{ \boldsymbol{\varepsilon}_n^m(k-1) \}\|. \quad (58)$$

Cause the matrices $\mathbf{P}_n^j(k)$ and $(\mathbf{C}_n)^T (\mathbf{B}_n^j(k))^{-1} \mathbf{C}_n$ are semi-definite, thus $\mathbf{f}_n^j(k)$ is stable. The transition matrix \mathbf{A} is time-invariant, so the estimation of model j , $\boldsymbol{\varepsilon}_n^j(k)$ is stable.

From equation (52), the total estimation error of node n is

$$E \{ \boldsymbol{\varepsilon}_n(k) \} = \sum_{j=1}^{L_n} \chi_n^j(k) E \{ \boldsymbol{\varepsilon}_n^j(k) \}, \quad (59)$$

which indicates that the estimation error of node n , $\boldsymbol{\varepsilon}_n(k)$ is stable. Hence, the proposed MFDKF can work stably and in an unbiased manner.

Then, the performance of consensus fusion is considered. After the consensus fusion, the expectation of estimation error is

$$E \{ \boldsymbol{\varepsilon}_n^c(k) \} = E \{ \boldsymbol{x}(k) - \hat{\boldsymbol{x}}_n^c(k) \}. \quad (60)$$

Substitute equation (48) (52) into equation (60) we have

$$E \{ \boldsymbol{\varepsilon}_n^c(k) \} = E \left\{ \boldsymbol{\varepsilon}_n(k) - \mathbf{C}_n \mathbf{A} \sum_{a_{mn}=1} (\boldsymbol{\varepsilon}_m(k-1) - \boldsymbol{\varepsilon}_n(k-1)) \right\}. \quad (61)$$

Since \mathbf{C}_n is a constant, \mathbf{A} is time-invariant, and $\boldsymbol{\varepsilon}_n(k)$ has previously been shown to be stable, $\boldsymbol{\varepsilon}_n^c(k)$ is stable.

5.2. Mean-Square Error Analysis

Firstly, the basic MFDKF is analyzed. The performance of mean-square error is determined by the estimation error covariance matrix, which is given by

$$E \{ \boldsymbol{\varepsilon}_n(k) (\boldsymbol{\varepsilon}_n(k))^T \} = \sum_{i=1}^{L_n} \sum_{j=1}^{L_n} \frac{\chi_n^i(k)}{\chi_n^j(k)} E \{ \boldsymbol{\varepsilon}_n^i(k) (\boldsymbol{\varepsilon}_n^j(k))^T \}, \quad (62)$$

Supposed that,

$$E \{ \boldsymbol{\varepsilon}_n^i(k) (\boldsymbol{\varepsilon}_n^j(k))^T \} = 0, i \neq j, \quad (63)$$

and denote that,

$$\begin{aligned} \boldsymbol{\Omega}_n^i(k) &= E \left\{ \boldsymbol{\varepsilon}_n^i(k) (\boldsymbol{\varepsilon}_n^i(k))^T \right\}, \\ \boldsymbol{\Omega}_n(k) &= E \left\{ \boldsymbol{\varepsilon}_n(k) (\boldsymbol{\varepsilon}_n(k))^T \right\}. \end{aligned} \quad (64)$$

Equation (62) could be expressed as

$$\boldsymbol{\Omega}_n(k) = \sum_{j=1}^{L_n} \boldsymbol{\Omega}_n^j(k). \quad (65)$$

From the representation in equation (53), $\boldsymbol{\Omega}_n^j(k)$ is calculated by

$$\boldsymbol{\Omega}_n^j(k) = \boldsymbol{\Gamma}_n^j(k) \sum_{i=1}^{L_n} \boldsymbol{\Omega}_n^i(k-1) (\boldsymbol{\Gamma}_n^i(k))^T + \boldsymbol{\Theta}_n^j(k), \quad (66)$$

where,

$$\begin{aligned}\Theta_n^j(k) &= \mathbf{f}_n^j(k) \mathbf{Q}(k) (\mathbf{f}_n^j(k))^T + \mathbf{K}_n^j(k) \mathbf{B}_n^j(k) (\mathbf{K}_n^j(k))^T, \\ \Gamma_n^j(k) &= \mathbf{f}_n^j(k) \mathbf{A}.\end{aligned}\quad (67)$$

Assume that $\mathbf{Q}(k)$, and $\mathbf{B}_n^j(k)$ are time-invariant, $\mathbf{f}_n^j(k)$, $\Theta_n^j(k)$, and $\Gamma_n^j(k)$ are time-invariant. As a result, $\Omega_n^j(k)$ are convergent. The time-invariant variables can be summarized as

$$\begin{aligned}\lim_{k \rightarrow \infty} \Omega_n^j(k) &= \Omega_n^j, \\ \lim_{k \rightarrow \infty} \Gamma_n^j(k) &= \Gamma_n^j, \\ \lim_{k \rightarrow \infty} \Theta_n^j(k) &= \Theta_n^j.\end{aligned}\quad (68)$$

By taking the limit of the equation (66),

$$\Omega_n^j = L_n \Gamma_n^j \Omega_n^j (\Gamma_n^j)^T + \Theta_n^j. \quad (69)$$

According to the rules of matrix vectorization as follows

$$\begin{aligned}vec(\mathbf{s}_1 \mathbf{s}_2 \mathbf{s}_3) &= (\mathbf{s}_3^T \otimes \mathbf{s}_1) vec(\mathbf{s}_2), \\ vec(\mathbf{s}_1 + \mathbf{s}_2) &= vec(\mathbf{s}_1) + vec(\mathbf{s}_2),\end{aligned}\quad (70)$$

equation (69) can be rewritten as

$$vec(\Omega_n^j) = L_n \Gamma_n^j \otimes \Gamma_n^j vec(\Omega_n^j) + vec(\Theta_n^j), \quad (71)$$

where \otimes is the Kronecker product. One can obtain the closed-form solution for equation (71)

$$vec(\Omega_n^j) = (\mathbf{I} - L_n \Gamma_n^j \otimes \Gamma_n^j)^{-1} vec(\Theta_n^j). \quad (72)$$

From equation (65) we know that the estimation error covariance matrix $\Omega_n(k)$ is the sum of the sub-models estimation error covariance matrix $\Omega_n^j(k)$. Thus, there exists a closed solution for the estimation error covariance matrix $\Omega_n(k)$.

Then the mean-square error of consensus fusion is considered. According to equation (61) the estimation error covariance matrix is written as

$$\begin{aligned}E \left\{ \boldsymbol{\varepsilon}_n^c(k) (\boldsymbol{\varepsilon}_n^c(k))^T \right\} &= \Omega_n(k) + \\ \mathbf{A} \sum_{a_{mn}=1} [\Omega_m(k-1) + \Omega_n(k-1)] \mathbf{A}^T.\end{aligned}\quad (73)$$

Its closed-form solution depends on $\Omega_n(k)$, whose closed-form solution exists.

6. Simulations

In this part, simulations are executed to validate the performance of the proposed MFDKF with its derived algorithms. Simulations in Section 6.1 are executed considering a linear system. To validate the MFDKF algorithm, the parameter is first set as its minimum value $\kappa = 2$, while compared with CDKF [16], DMCKF [35], DMEEKF [39], and BIKF [40]. Then, the value of parameter κ is in discussion. In Section 6.2, a linear target tracking model is considered to further verify the performance of MFDKF. Specific scenarios are considered in Section 6.3, where the performance of derived C-MFDKF and S-MFDKF are shown.

Without special instructions, each simulation in this paper is implemented with 500 independent Monte Carlo runs, and 1000 samples are utilized to calculate the RMSE of the estimations. The RMSE to measure the accuracy is calculated by

$$RMSE = \sqrt{\frac{\sum_{k=1}^{N_1} (\|\hat{\mathbf{x}}(k) - \mathbf{x}(k)\|^2)}{N_1}}, \quad (74)$$

where $\hat{\mathbf{x}}(k)$ and $\mathbf{x}(k)$ severally denotes the estimated state and true state in k -th run. N_1 is the number of Monte Carlo runs. Simulations are implemented under Gaussian noise and some non-Gaussian noises (mixed Gaussian, α -stable) as below.

1. The noise obeying Gaussian distribution is described as

$$\mathbf{v} \sim \mathcal{N}(\mu, \sigma), \quad (75)$$

where $\mathcal{N}(\mu, \sigma)$ represents Gaussian distribution with mean μ and variance σ .

2. The noise obeying mixed Gaussian distribution is described as

$$\mathbf{v} \sim \lambda \mathcal{N}(\mu, \sigma_1) + (1 - \lambda) \mathcal{N}(\mu, \sigma_2), \quad (76)$$

where λ is the mixed coefficient of two Gaussian noises. The noise obeys this kind of mixed Gaussian distribution is denoted as $\mathbf{v} \sim \mathcal{M}(\lambda, \mu, \sigma_1, \sigma_2)$.

3. The α -stable distribution is described as following characteristic function

$$\phi(t) = \exp \{j\varpi t - \zeta|t|^a [1 + jbsign(t)\omega(t, a)]\}, \quad (77)$$

with

$$\omega(t, a) = \begin{cases} \tan\left(\frac{a\pi}{2}\right), & a \neq 1, \\ \frac{2}{\pi} \log|t|, & a = 1. \end{cases} \quad (78)$$

a denotes the characteristic exponent, b is the symmetry parameter, ζ and ϖ severally represent the dispersion parameter and the location parameter. $|\cdot|$ in this function denotes the absolute value operation. The noise that follows this kind of distribution is expressed as $\mathbf{v} \sim \mathcal{S}(a, b, \zeta, \varpi)$.

The following simulations are played on the WSN whose communication typology is shown in Fig. 3.

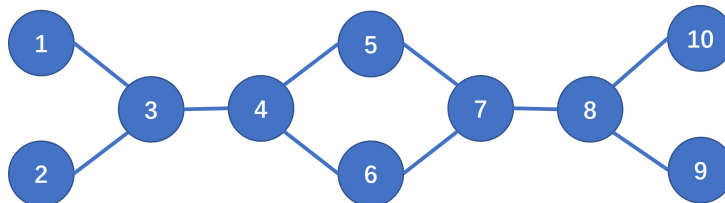


Figure 3: Communication typology of WSN

6.1. A linear system

In this section, the following linear system is considered [35]

$$\mathbf{x}(k) = \begin{bmatrix} \cos(\theta) & -\sin(\theta) \\ \sin(\theta) & \cos(\theta) \end{bmatrix} \mathbf{x}(k-1) + \mathbf{w}(k-1), \quad (79)$$

$$\mathbf{z}_n(k) = \begin{bmatrix} 1 & 1 \end{bmatrix} \mathbf{x}(k) + \mathbf{v}_n(k), \quad (80)$$

where, $\theta = \pi/18$. $\mathbf{w}(k)$ and $\mathbf{v}_n(k)$ severally denotes the transition noise and observation noise. The initial values of $\mathbf{x}(0)$, $\hat{\mathbf{x}}(0)$ and $\mathbf{M}(0)$ are set to

$$\begin{aligned} \mathbf{x}(0) &= \mathbf{I}^{p \times 1}, \\ \hat{\mathbf{x}}(0) &= \mathbf{x}(0), \\ \mathbf{M}(0) &= \mathbf{I}^{p \times p}. \end{aligned} \quad (81)$$

The process noise obeys Gaussian noise as bellow

$$\mathbf{w}(k) \sim \mathcal{N}(0, 0.1). \quad (82)$$

The node 4 whose neighbors are node 3, 5, 6 was considered to compare the performance of MFDKF with CDKF, DMCKF, DMEEKF, and BIKF.

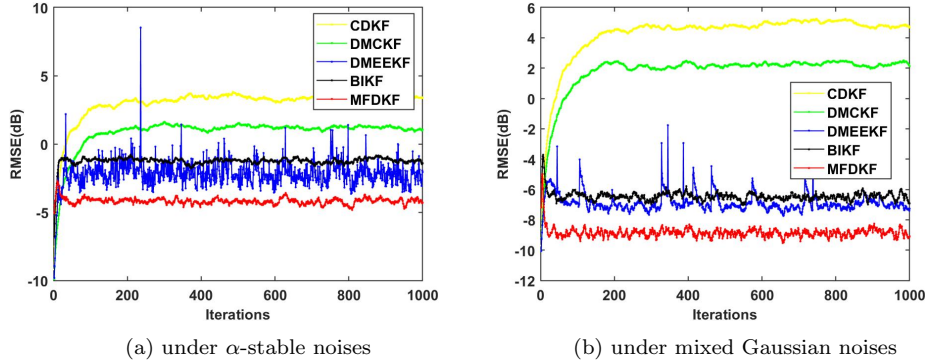


Figure 4: Fig. 4a and Fig. 4b shows the RMSEs of the algorithms (CDKF, DMCKF, DMEEKF, BIKF, MFDKF) when the observation noise is the α -stable distribution as model (83) and the Gaussian distribution as model (84), respectively.

First, the MFDKF with minimum parameter value $\kappa = 2$ is considered. We set the observation noise of each node as following α -stable noise

$$\mathbf{v}(k) \sim \mathcal{S}(1.2, 0, 2, 0). \quad (83)$$

The kernel bandwidth of DMCKF and DMEEKF is set to $\sigma_{DMCKF} = 1$ and $\sigma_{DEEKF} = 0.5$ respectively, which works relatively better in the situation. The RMSE performance of the algorithms is shown in Fig. 4a, from which we can conclude that the MFDKF accomplishes the estimation with the minimum RMSEs and the best stability. The second best is the DMEEKF, which has a large jitter in the RMSEs. As for the RMSE performance of the rest algorithms, they are BIKF, DMCKF, and CDKF in descending order. The specific value of the simulations is listed in Table 4a. Subsequently, the observation noise is set as following mixed Gaussian distribution

$$\mathbf{v}(k) \sim \mathcal{M}(0.9, 0, 100^2, 1). \quad (84)$$

The kernel bandwidth of DMCKF and DMEEKF are set in a proper value $\sigma_{DMCKF} = 1$ and $\sigma_{DEEKF} = 0.5$, respectively. Fig. 4b shows the MFDKF

works stably with the best accuracy while some abnormal estimations occur in the DMEEKF. And the detailed values are presented in Table 4b. The simulations mentioned above verified the B-MFDKF outperforms the CDKF, MDCKF, DMEEKF, and BIKF while the observation noise are obey some non-Gaussian distribution.

Table 4: Table 4a, Table 4b and Table 4c show the RMSE of the algorithms (CDKF, DMCKF, DMEEKF, BIKF, MFDKF) when the observation noises are α -stable distribution as (83), mixed Gaussian distribution as (84) and Gaussian distributed as (85), respectively.

Filters	RMSE (m)	Filters	RMSE (m)	Filters	RMSE (m)
CDKF	1.43	CDKF	1.65	CDKF	0.35
DMCKF	1.11	DMCKF	1.24	DMCKF	0.35
DMEEKF	0.78	DMEEKF	0.45	DMEEKF	0.36
BIKF	0.87	BIKF	0.48	BIKF	0.46
MFDKF	0.62	MFDKF	0.36	MFDKF	0.35

(a)
(b)
(c)

Then, the following Gaussian noise is considered

$$\mathbf{v}(k) \sim \mathcal{N}(0, 1). \quad (85)$$

Fig. 5a shows the RMSEs of the five algorithms, while $\sigma_{DMCKF} = \sigma_{DEEKF} = 100$. It's easy to see that the performance of MFDKF is as good as CDKF, DMCKF, and DMEEKF, while BIKF performs less outstandingly. More details are shown in Table 4c.

To prove the improvement of the proposed MFDKF, we consider different non-Gaussian noises (including the α -stable noise and the mixed Gaussian noise) as the observation noise in this linear model, the results are shown in Table 5. We can see that MFDKF outperforms other algorithms under some non-Gaussian observation environments.

The performance of different nodes in the WSN is considered when the observation noise obeys the distribution as (83). Table 6 shows the RMSE of different nodes in the WSN as shown in Fig. 3. By analyzing Table 6, it can be concluded that the more neighbors a node have, the more accurate its estimation is. Note that the more neighbors a node have, the larger its degree value and the more observation sub-models the MFDKF needs to fuse. That is, the more neighbors there are, the larger L_n is, and the greater the computational complexity of the MFDKF.

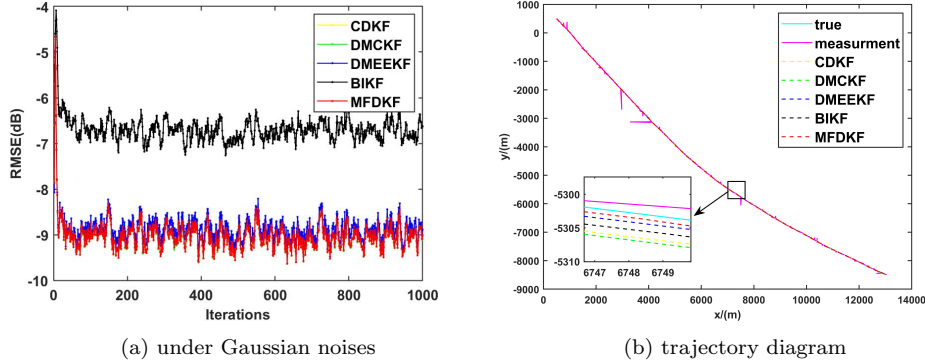


Figure 5: Fig. 5a shows the RMSEs of the algorithms (CDKF, DMCKF, DMEEKF, BIKF, MFDKF) when the observation noise is the Gaussian distribution as (85). Fig. 5b shows the target tracking trajectory diagram of the five algorithms.

Table 5: RMSEs under different non-Gaussian noises (a linear system)

Noises distribution	RMSE of the algorithms (m)				
	CDKF	DMCKF	DMEEKF	BIKF	B-MFDKF
$\mathcal{S}(1.2, 0, 0.5, 0)$	0.73	0.58($\sigma = 6$)	0.42($\sigma = 2$)	0.46	0.35
$\mathcal{S}(1.2, 0, 3, 0)$	1.73	1.33($\sigma = 2$)	1.11($\sigma = 1$)	1.06	0.75
$\mathcal{S}(1.5, 0, 0.5, 0)$	0.45	0.37($\sigma = 3$)	0.36($\sigma = 2$)	0.43	0.33
$\mathcal{S}(1.5, 0, 3, 0)$	1.07	0.87($\sigma = 3$)	0.90($\sigma = 2$)	0.98	0.7
$\mathcal{M}(0.9, 0, 50^2, 1)$	1.22	0.90($\sigma = 1$)	0.49($\sigma = 1$)	0.48	0.36
$\mathcal{M}(0.9, 0, 100^2, 5^2)$	1.70	1.32($\sigma = 1$)	1.04($\sigma = 1$)	1.04	0.74
$\mathcal{M}(0.8, 0, 50^2, 1)$	1.43	1.12($\sigma = 1$)	1.01($\sigma = 1$)	0.49	0.37
$\mathcal{M}(0.8, 0, 100^2, 5^2)$	1.97	1.59($\sigma = 1$)	2.05($\sigma = 1$)	1.06	0.76

Table 6: RMSEs of different nodes in the WSN

Node	1	2	3	4	5	6	7	8	9	10
Degree: d_n	2	3	3	4	3	3	4	4	2	1
RMSE (m)	0.73	0.73	0.62	0.62	0.67	0.66	0.62	0.62	0.73	0.73

At the end of this section, we compare the performance of MFDKF with different values of parameter κ . The observation noises are set as an alpha-stable noise denoted by (83). And the results of EM algorithms with different κ for noise approximation are shown in Table 7.

As shown in Table 8, increasing κ improves the performance of MFDKF. It is due to the increasing κ improved the noise estimation from the EM algo-

Table 7: Noise approximation by EM algorithm

κ	$\mathbf{R}^i(k)$	$\gamma^i(t)$
1	3.28×10^3	1
2	$(5.56 \times 10^4, 18.76)$	(0.06, 0.94)
3	$(1.21 \times 10^5, 1.2 \times 10^2, 5.4)$	(0.03, 0.26, 0.71)
4	$(1.5 \times 10^5, 2.27 \times 10^2, 20.4, 3.46)$	(0.02, 0.16, 0.32, 0.5)
5	$(3.77 \times 10^5, 1.55 \times 10^3, 57.36, 7.53, 3.22)$	(0.01, 0.06, 0.29, 0.26, 0.38)

rithm. In other words, the increasing κ enables the fusion observation model to be approximated more precisely by observation sub-models. However, the performance of the proposed MFDKF cannot be improved indefinitely by increasing the parameter κ . As κ increases, the performance of the MFDKF improves less and less, and the algorithm fails to converge when $\kappa = 6$. Because, with the increase of κ , the estimation of noise by the EM algorithm approaches its limit, i.e., the approximation of the fusion observation model tends to its limit.

Table 8: RMSEs of the MFDKF with different values of κ

κ	2	3	4	5
L_n	16	64	256	1024
RMSE (m)	0.538	0.496	0.49	0.489

As shown in Table 8, the value of L_n increases exponentially with the increase of κ , which means the computation complexity increases exponentially. If a particularly high estimation accuracy is not required, $\kappa = 2$ is the best choice. Therefore, in the following simulations, we only consider $\kappa = 2$ for the MFDKF and its derived algorithms.

6.2. Target tracking system

To further validate the MFDKF algorithm, the following target tracking system [36] is considered

$$\begin{aligned} \mathbf{x}(k) &= \mathbf{A}\mathbf{x}(k-1) + \mathbf{G}\mathbf{w}(k-1), \\ \mathbf{z}_n(k) &= \mathbf{H}\mathbf{x}(k) + \mathbf{v}_n(k), \end{aligned} \tag{86}$$

where,

$$\mathbf{A} = \begin{bmatrix} 1 & 1 & 0 & 0 \\ 0 & 1 & 0 & 0 \\ 0 & 0 & 1 & 1 \\ 0 & 0 & 0 & 1 \end{bmatrix}, \mathbf{G} = \begin{bmatrix} \frac{1}{2} & 1 & 0 & 0 \\ 0 & 0 & \frac{1}{2} & 1 \end{bmatrix}, \mathbf{H} = \begin{bmatrix} 1 & 0 & 0 & 0 \\ 0 & 0 & 1 & 0 \end{bmatrix} \quad (87)$$

The process noise is set as a Gaussian noise

$$\mathbf{w}(k) \sim \mathcal{N}(\mathbf{0}, \mathbf{Q}), \mathbf{Q} = \begin{bmatrix} 0.1^2 & 0 \\ 0 & 0.1^2 \end{bmatrix}. \quad (88)$$

Here, $\mathbf{x}(k) = [x_1 \ x_2 \ x_3 \ x_4]^T$ is the state vector of the target, x_1 and x_3 represent the position in the x and y directions, x_2 and x_4 represent the velocity in the x and y directions. And the initial values of $\mathbf{x}(0)$, $\hat{\mathbf{x}}(0)$, and $\mathbf{M}(0)$ are set to

$$\begin{aligned} \mathbf{x}(0) &= [500, 10, 500, -10]^T, \\ \mathbf{M}(0) &= \mathbf{I}^{p \times p}, \\ \hat{\mathbf{x}}(0) &= \mathbf{x}(0). \end{aligned} \quad (89)$$

Similar to Section 6.1, we compare the performance of MFDKF ($\kappa = 2$) with CDKF, DMCKF, DMEEKF, and BIKF by considering node 4 in the WSN as shown in Fig. 3.

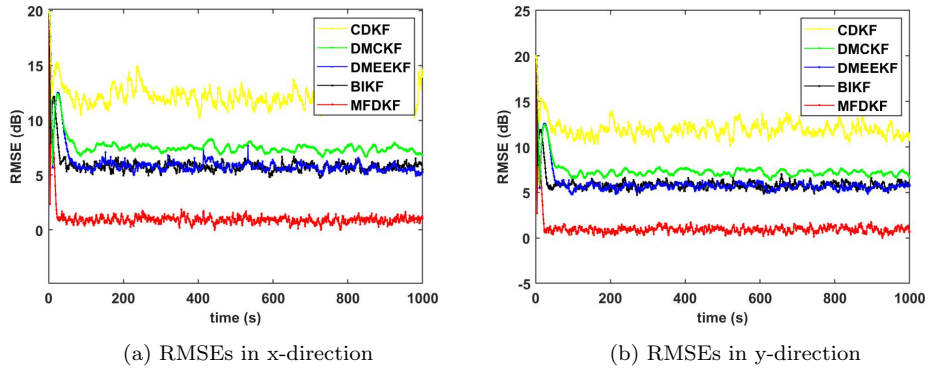


Figure 6: Fig. 6a and Fig. 6b severally show the RMSEs positioned in the x and y directions.

Firstly, the α -stable noise denoted by (83) is considered. Fig. 5b shows trajectories of the position estimation with the five algorithms when the kernel bandwidths of DMCKF and DMEEKF are $\sigma_{DMCKF} = 1$ and $\sigma_{DEEKF} =$

1.5 respectively. The trajectories show the proposed MFDKF is able to achieve a more accurate target location estimation. Fig. 6 shows RMSEs in the x and y directions. One can manifest that the proposed MFDKF works with the smallest steady-state error and perform stably, while the DMEEKF and BIKF come second. The RMSE of DMCKF is slightly larger than DMEEKF and that of CDKF is largest. The details can be found in Table 9.

Table 9: RMSEs of x and y direction under different noises distributions

Noises distribution	(RMSE of x direction (m), RMSE of y direction (m))				
	CDKF	DMCKF	DMEEKF	BIKF	MFDKF
$S(1.2, 0, 2, 0)$	(4.08,3.99)	(2.43,2.37)	(2.04,2.02)	(2,2)	(1.15,1.15)
$M(0.9, 0, 100^2, 1)$	(5.17,5.19)	(2.81,2.82)	(2.22,2.23)	(1.21,1.11)	(0.42,0.42)
$N(0, 1)$	(0.35,0.36)	cannot work	(0.5,0.5)	(0.62,0.623)	(0.36,0.36)

Secondly, the mixed Gaussian noises denoted by (84) are considered as the observation noises. And the kernel bandwidth of DMCKF and DMEEKF remains unchanged. The RMSE results are shown in Table 9, which shows that the proposed MFDKF works with the smallest state error of all the five algorithms.

Subsequently, we consider the observation noises are Gaussian distribution as (85). The target tracking error of the five algorithms in x and y directions are shown in Tabel 9. One can conclude that the proposed MFDKF can almost work as well as CDKF, while the BIKF and DMEEKF are working with larger errors. And the DMCKF even cannot work without adjusting the kernel bandwidth.

To prove the improvement of the proposed MFDKF in target tracking (CV model), different non-Gaussian noises (including the α -stable noise and the mixed Gaussian noise) are considered as the observation noise. The results are shown in Table 10, when the kernel bandwidth of DMCKF and DMEEKF remain as $\sigma_{DMCKF} = 1$ and $\sigma_{DEEKF} = 1.5$. Within expectation, the CDKF cannot handle some non-Gaussian noise as shown in Table 10. Comparatively, the DMCKF and DMEEKF perform better but are unstable because the parameters σ_{DMCKF} and σ_{DEEKF} need to be adjusted accordingly. The proposed MFDKF performs best with all cases in the table, which indicate its capability and stability.

Table 10: RMSEs of x and y directions under the different noises

Noises distribution	(RMSE of x direction (m), RMSE of y direction (m))				
	CDKF	DMCKF	DMEEKF	BIKF	MFDKF
$S(1.2, 0, 0.5, 0)$	(1.35,1.39)	(0.83,0.85)	(0.69,0.72)	(0.8122,0.7925)	(0.4,0.4)
$S(1.2, 0, 3, 0)$	(5.4,5.45)	(3.23,3.26)	(2.74,2.74)	(2.69,2.74)	(1.55,1.56)
$S(1.5, 0, 0.5, 0)$	(0.6,0.58)	cannot work	(0.38,0.37)	(0.64,0.66)	(0.33,0.33)
$S(1.5, 0, 3, 0)$	(2.48,2.45)	(1.83,1.84)	(1.69,1.69)	(2.25,2.27)	(1.31,1.32)
$M(0.9, 0, 50^2, 1)$	(3.07,3.08)	(1.68,1.70)	(1.35,1.37)	(0.89,0.89)	(0.43,0.42)
$M(0.9, 0, 100^2, 5^2)$	(5.21,5.22)	(2.99,3.02)	(2.47,2.49)	(2.44,2.44)	(1.42,1.42)
$M(0.8, 0, 50^2, 1)$	(4.01,4.01)	(2.43,2.43)	(2.1,2.13)	(1.16,1.25)	(0.51,0.51)
$M(0.8, 0, 100^2, 5^2)$	(6.74,6.75)	(4.19,4.2)	(3.74,3.75)	(2.78,2.77)	(1.58,1.58)

6.3. Simulation of C-MFDKF and S-MFDKF

The simulations above indicated the improvement of the proposed MFDKF. Here, we discuss the performance of its derived algorithms under specific situations (take $\kappa = 2$ as an example). The disagreement between nodes in WSN is represented by

$$\delta = \sqrt{\sum_{n=1}^{N_2} \|\hat{\mathbf{x}}_n(k) - \boldsymbol{\mu}(k)\|^2}, \quad (90)$$

$$\boldsymbol{\mu}(k) = \frac{1}{N_2} \sum_{n=1}^{N_2} \hat{\mathbf{x}}_n(k),$$

where N_2 indicates the total number of nodes. It reflects the consensus of all nodes in the WSN, and a smaller value indicates a more consistent result between nodes.

In the first situation, consider a WSN that has a high demand for consensus between each sensor node. Assume that there are no restrictions on communication between neighboring nodes so that all information interactions in C-MFDKF can be satisfied.

Take the linear system in Section 6.1 as an example, and the observation noises are set as the α -stable noise denoted by (83). The RMSEs and disagreements of the basic C-MFDKF ($\kappa = 2$) with different values of ξ are shown in Fig. 7a and Fig. 7b. From the performances, we can conclude that C-MFDKF can effectively reduce the disagreement between nodes while ensuring the accuracy of estimation. The larger the value of ξ , the better the consistency of C-MFDKF estimation while improving accuracy. The details of the simulation are shown in Table 11.

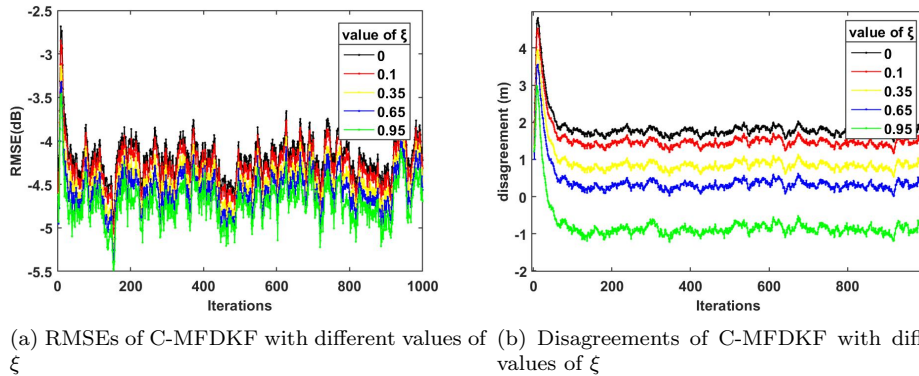


Figure 7: Fig. 7a and Fig. 7b show the RMSEs and the disagreement performances of the C-MFDKF with different values of ξ , respectively.

Table 11: RMSEs and disagreements of C-MFDKF with different ξ

ξ	0	0.1	0.35	0.65	0.95
REMS (m)	0.62	0.61	0.6	0.59	0.58
Disagreement (m)	1.24	1.19	1.11	1.05	0.91

Considered a situation that the WSN has limitations in terms of information interaction between neighboring nodes. Assume that the communication capability between neighboring nodes is only sufficient to exchange LKF results with each other. In these circumstances, the MFDKF cannot work since it needs to use the observations of its neighboring nodes.

Take the target tracking model in Section 6.2 as an example, and set the observation noise as the mixed Gaussian distribution (84). The performances of S-MFDKF with different parameters ξ are compared. Table 12 shows that both the accuracy and the consensus are improved compared to BIKF without communication.

Table 12: RMSEs and disagreements of S-MFDKF with different ξ

ξ	RMSE (m)				Disagreement (m)			
	0	0.2	0.4	0.6	0	0.2	0.4	0.6
X direction	1.18	1.07	1.01	1.02	2.32	2.08	1.94	2
Y direction	1.18	1.07	1.01	1.02	2.33	0.66	0.62	0.62

7. Conclusion

In this work, a MFDKF has been proposed for the WSNs in which the observation noise exhibits non-Gaussian characteristics. The proposed MFDKF approximates the observation noise as GMM utilizing the EM algorithm. Based on this, the observation model of DKF can be modeled as a combination of sub-models with different Gaussian components. The final estimation is achieved by fusing all sub-models with the IMM. Considering WSNs with high consensus requirements and low communication capabilities, consensus rule-based C-MFDKF and S-MFDKF were proposed, respectively. The mean error analysis and mean-square error analysis are given to verify the convergence of the proposed MFDKF and its derived algorithms. Simulations on the simple linear system, and target tracking system (cv model), validated the desirable performance of the proposed MFDKF and its derived algorithms.

The limitation of our proposed MFDKF is that the computational complexity increases exponentially as the number of its neighbors increases. It means that the proposed MFDKF and its derived algorithms are unsuitable for large WSNs. Additionally, adequate and accurate samples of observation noise are essential for the proposed algorithms, which is the basis for noise approximation before the state estimation.

In the future, the proposed MFDKF can be considered for derivation to nonlinear systems.

8. Acknowledges

This study was founded by the National Natural Science Foundation of China under Grant No.51975107, the Sichuan Science and Technology Major Project No.2022ZDZX0039, No.2019ZDZX0020, and the Sichuan Science and Technology Program No.2022YFG0343.

References

- [1] M. Ma, B. He, N. Wang, R. Shen, A method for monitoring the solar resources of high-scale photovoltaic power plants based on wireless sensor networks, *Sustainable Energy Technologies and Assessments* 53 (2022) 102678.

- [2] C. Zhang, J. Qin, H. Li, Y. Wang, S. Wang, W. X. Zheng, Consensus-based distributed two-target tracking over wireless sensor networks, *Automatica* 146 (2022) 110593.
- [3] B. Jia, K. D. Pham, E. Blasch, D. Shen, Z. Wang, G. Chen, Cooperative space object tracking using space-based optical sensors via consensus-based filters, *IEEE Transactions on Aerospace and Electronic Systems* 52 (4) (2016) 1908–1936.
- [4] Z. Zhang, Y. Zhang, Application of wireless sensor network in dynamic linkage video surveillance system based on kalman filtering algorithm, *The Journal of Supercomputing* 75 (2019) 6055–6069.
- [5] V. Vahidpour, A. Rastegarnia, A. Khalili, S. Sanei, Partial diffusion kalman filtering for distributed state estimation in multiagent networks, *IEEE transactions on neural networks and learning systems* 30 (12) (2019) 3839–3846.
- [6] R. Wang, B. Chen, Z. Hu, D. W. Ho, L. Yu, Distributed event-triggered fusion estimation for networked asynchronous multi-rate systems, *Information Fusion* (2023) 101846.
- [7] H.-S. Shin, S. He, A. Tsourdos, Sample greedy gossip distributed kalman filter, *Information Fusion* 64 (2020) 259–269.
- [8] S. He, H.-S. Shin, S. Xu, A. Tsourdos, Distributed estimation over a low-cost sensor network: A review of state-of-the-art, *Information Fusion* 54 (2020) 21–43.
- [9] S. Sun, H. Lin, J. Ma, X. Li, Multi-sensor distributed fusion estimation with applications in networked systems: A review paper, *Information Fusion* 38 (2017) 122–134.
- [10] S.-L. Sun, Z.-L. Deng, Multi-sensor optimal information fusion kalman filter, *Automatica* 40 (6) (2004) 1017–1023.
- [11] J. Sijs, M. Lazar, P. Van den Bosch, Z. Papp, An overview of non-centralized kalman filters, in: *2008 IEEE International Conference on Control Applications*, IEEE, 2008, pp. 739–744.

- [12] T. Li, J. M. Corchado, J. Prieto, Convergence of distributed flooding and its application for distributed bayesian filtering, *IEEE Transactions on Signal and Information Processing over Networks* 3 (3) (2016) 580–591.
- [13] X. Yang, W.-A. Zhang, L. Yu, A bank of decentralized extended information filters for target tracking in event-triggered wsns, *IEEE Transactions on Systems, Man, and Cybernetics: Systems* 50 (9) (2019) 3281–3289.
- [14] T. Li, J.-F. Zhang, Mean square average-consensus under measurement noises and fixed topologies: Necessary and sufficient conditions, *Automatica* 45 (8) (2009) 1929–1936.
- [15] L. Ma, Z. Wang, Q.-L. Han, Y. Liu, Consensus control of stochastic multi-agent systems: a survey, *Science China Information Sciences* 60 (2017) 1–15.
- [16] R. Olfati-Saber, Kalman-consensus filter: Optimality, stability, and performance, in: *Proceedings of the 48th IEEE Conference on Decision and Control (CDC) held jointly with 2009 28th Chinese Control Conference, Ieee, 2009*, pp. 7036–7042.
- [17] R. Olfati-Saber, Distributed kalman filtering for sensor networks, in: *2007 46th IEEE Conference on Decision and Control, IEEE, 2007*, pp. 5492–5498.
- [18] R. Olfati-Saber, Distributed kalman filter with embedded consensus filters, in: *Proceedings of the 44th IEEE Conference on Decision and Control, IEEE, 2005*, pp. 8179–8184.
- [19] J. Wang, J. Li, S. Yan, W. Shi, X. Yang, Y. Guo, T. A. Gulliver, A novel underwater acoustic signal denoising algorithm for gaussian/non-gaussian impulsive noise, *IEEE Transactions on Vehicular Technology* 70 (1) (2020) 429–445.
- [20] T. Guzel, E. Ustunel, H. B. Celebi, H. Delic, K. Mihcak, Noise modeling and ofdm receiver design in power-line communication, *IEEE Transactions on Power Delivery* 26 (4) (2011) 2735–2742.

- [21] K. Jahan, S. K. Rao, Implementation of underwater target tracking techniques for gaussian and non-gaussian environments, *Computers & Electrical Engineering* 87 (2020) 106783.
- [22] Y. Fu, M. Sun, Y. Gao, Tightly coupled distributed kalman filter under non-gaussian noises, *Signal Processing* 200 (2022) 108678.
- [23] J. He, G. Wang, H. Yu, J. Liu, B. Peng, Generalized minimum error entropy kalman filter for non-gaussian noise, *ISA transactions* (2022).
- [24] J. He, G. Wang, X. Zhang, H. Wang, B. Peng, Maximum total generalized correntropy adaptive filtering for parameter estimation, *Signal Processing* 203 (2023) 108787.
- [25] B. Ristic, S. Arulampalam, N. Gordon, *Beyond the Kalman filter: Particle filters for tracking applications*, Artech house, 2003.
- [26] D. Gu, Distributed particle filter for target tracking, in: *Proceedings 2007 IEEE International Conference on Robotics and Automation*, IEEE, 2007, pp. 3856–3861.
- [27] J. Read, K. Achutegui, J. Miguez, A distributed particle filter for non-linear tracking in wireless sensor networks, *Signal Processing* 98 (2014) 121–134.
- [28] J. Y. Yu, M. J. Coates, M. G. Rabbat, S. Blouin, A distributed particle filter for bearings-only tracking on spherical surfaces, *IEEE Signal Processing Letters* 23 (3) (2016) 326–330.
- [29] J. Li, A. Nehorai, Distributed particle filtering via optimal fusion of gaussian mixtures, *IEEE Transactions on Signal and Information Processing over Networks* 4 (2) (2017) 280–292.
- [30] C. Xu, S. Zhao, B. Huang, F. Liu, Distributed student’s t filtering algorithm for heavy-tailed noises, *International Journal of Adaptive Control and Signal Processing* 32 (6) (2018) 875–890.
- [31] B. Chen, X. Liu, H. Zhao, J. C. Principe, Maximum correntropy kalman filter, *Automatica* 76 (2017) 70–77.

- [32] B. Chen, L. Dang, Y. Gu, N. Zheng, J. C. Príncipe, Minimum error entropy kalman filter, *IEEE Transactions on Systems, Man, and Cybernetics: Systems* 51 (9) (2019) 5819–5829.
- [33] G. Wang, B. Chen, X. Yang, B. Peng, Z. Feng, Numerically stable minimum error entropy kalman filter, *Signal Processing* 181 (2021) 107914.
- [34] J. He, G. Wang, K. Cao, H. Diao, G. Wang, B. Peng, Generalized minimum error entropy for robust learning, *Pattern Recognition* 135 (2023) 109188.
- [35] G. Wang, R. Xue, J. Wang, A distributed maximum correntropy kalman filter, *Signal Processing* 160 (2019) 247–251.
- [36] C. Hu, B. Chen, An efficient distributed kalman filter over sensor networks with maximum correntropy criterion, *IEEE Transactions on Signal and Information Processing over Networks* 8 (2022) 433–444.
- [37] W. Liu, P. P. Pokharel, J. C. Principe, Correntropy: Properties and applications in non-gaussian signal processing, *IEEE Transactions on signal processing* 55 (11) (2007) 5286–5298.
- [38] Y. Zhang, B. Chen, X. Liu, Z. Yuan, J. C. Principe, Convergence of a fixed-point minimum error entropy algorithm, *Entropy* 17 (8) (2015) 5549–5560.
- [39] Z. Feng, G. Wang, B. Peng, J. He, K. Zhang, Distributed minimum error entropy kalman filter, *Information Fusion* 91 (2023) 556–565.
- [40] X. Fan, G. Wang, J. Han, Y. Wang, A background-impulse kalman filter with non-gaussian measurement noises, *IEEE Transactions on Systems, Man, and Cybernetics: Systems* (2022).
- [41] D. A. Reynolds, Gaussian mixture models., *Encyclopedia of biometrics* 741 (659-663) (2009).
- [42] I. Bilik, J. Tabrikian, Maneuvering target tracking in the presence of glint using the nonlinear gaussian mixture kalman filter, *IEEE Transactions on Aerospace and Electronic Systems* 46 (1) (2010) 246–262.

- [43] Z. Min, J. Wang, M. Q.-H. Meng, Robust generalized point cloud registration with orientational data based on expectation maximization, *IEEE Transactions on Automation Science and Engineering* 17 (1) (2019) 207–221.
- [44] F. Guo, O. Wu, H. Kodamana, Y. Ding, B. Huang, An augmented model approach for identification of nonlinear errors-in-variables systems using the em algorithm, *IEEE Transactions on Systems, Man, and Cybernetics: Systems* 48 (11) (2017) 1968–1978.
- [45] X. Fan, G. Wang, J. Han, Y. Wang, Interacting multiple model based on maximum correntropy kalman filter, *IEEE Transactions on Circuits and Systems II: Express Briefs* 68 (8) (2021) 3017–3021.
- [46] G. Xie, L. Sun, T. Wen, X. Hei, F. Qian, Adaptive transition probability matrix-based parallel imm algorithm, *IEEE Transactions on Systems, Man, and Cybernetics: Systems* 51 (5) (2019) 2980–2989.